Chapter-6

Pyrolysis behavior of low value biomass (*Sesbania bispinosa*) to elucidate its bioenergy potential: Kinetic, thermodynamic and pyrolysis factor optimization based on response surface methodology

6.1 Introduction

Dhaincha (*Sesbania bispinosa*), also known as *Sesbania aculeata*, is found widely in Asian and North African countries. It is grown mostly as green manure, domestic fuel, and fodder in India. It grows quickly in different types of soil, such as waterlogged, sandy, saline, and clay soil. It is succulent, has lower water requirements, and produces a high amount of organic matter and nitrogen in the soil. It can reach upto a height of 7m, matures in 150 days, and produces 14 tons per acre on average.

Reaction factors, such as temperature, heating rate, inert gas flow rate, residence time, etc., directly impact biomass pyrolysis. However, it is also dependent on the biomass characteristic and content. A detailed, comprehensive study is necessary throughout the bioenergy product development process to efficiently utilize any biomass to understand the kinetics and reaction conditions. Furthermore, each biomass decomposes at a specific temperature. Even the mineral matter content of the same type of biomass will vary depending on the type of soil and climatic circumstances under which it is cultivated. As a consequence, kinetic parameters might vary even for the same biomass obtained from different geographical locations.

The main motive in selecting *Sesbania bispinosa* for elucidating its bioenergy potential was its fast growth and wide availability. Thus the present work was carried out to acknowledge the physicochemical characterization, thermal degradation behavior, and optimizing the pyrolysis process variables. The model-free approaches of Ozawa Flynn Wall (OFW), Kissinger Akahira Sunose (KAS), Tang (TM), Starink (ST), and Vyazovkin (VZK) were used to compute the kinetic parameters. Criado $z(\alpha)$ master plot method was used to determine the reaction mechanism. The nature of the reaction was also computed using thermodynamic study. A laboratory-based cylindrical-shaped reactor was used to perform the thermal pyrolysis experiment. The influence of process factors (temperature, heating rate, and N_2 flow rate) was optimized using RSM based on CCD. The pyrolytic products (liquid and solid) gained were characterized via

proximate, ultimate analysis, FTIR, GCMS, viscosity, density, pH, heating value (HHV), moisture content, etc.

6.2 Physicochemical characterization of SB

Proximate analysis such as moisture content, volatile matter, and ash content was carried out in accordance with ASTM standards (E 871, E 872, and E1755), while fixed carbon was calculated on a difference basis. Elemental analysis such as C, H, N, and S was carried out with an elemental analyzer (Euro, EA, Germany), while oxygen was calculated on a difference basis. A bomb calorimeter (Rajdhani Scientific Instrument Company, New Delhi, India) was used to determine the higher heating value (HHV). A digital balance and graduated cylinder were used to determine the bulk density. The hemicellulose, cellulose, and lignin content (fiber analysis) were determined using the method reported in section 3.2.7. FTIR analysis (FTIR, Model: Nicolet iS5) in the wavelength range (400 – 4000 cm^{-1}) was used to determine the functional groups linked to the SB biomass. The biomass was uniformly mixed with KBr at a ratio of 1:100, and scanning was performed at the rate of 40 with a step size of 4 cm^{-1}.

6.3 Thermogravimetric analysis (TGA)

SB was thermally analyzed in a thermogravimetric analyzer (Shimadzu, Singapore, TGA 50) at 10 °C/min under inert nitrogen (100 ml/min) conditions from room temperature to 1000°C. Further, the same TGA instrument was used for pyrolysis of the SB biomass at dynamic heating rates of 10, 20, 30, 40, and 50 °C/min.

6.4 Design of experiments (DOE)

Process variables are directly linked to the yield and properties of the pyrolysis product. Heating rate, temperature, and N_2 flow rate are the important factors deciding the yield of the pyrolysis product. As a result, optimizing these process variables prior to the experimentation becomes critical. The current study is based on optimizing critical pyrolysis factors such as temperature, heating rate, and N_2 flow rate (coded as A, B, and C) respectively as independent

variables, whereas bio-oil yield was selected as a dependent variable employing a design expert (DE) software (Statease USA, 11) based on central composite design (CCD). This approach is extensively used because it requires a small number of operations to optimize the response variable. It gives an easy way to evaluate the interactions between several factors. A total of 19 trials has been performed as given by the design expert software, consisting of 6, 8, and 5 axial, factorial, and center points, respectively, replicates at five distinct points (-alpha, +alpha, -1, +1, 0), can also be assessed from Eq. (6.1) below.

$$N = 2^n + 2n + n_c = 2^3 + 2 \times 3 + 5 = 19 \quad (6.1)$$

where N is the total number of trials to be done, n denotes the number of independent variables, and n_c denotes the number of repetitions at center locations. All the experimental results were fitted into a 2nd-degree model equation.

$$Y = \beta_o + \sum_{i=1}^{n} \beta_i X_i + \sum_{i=1}^{n} \beta_{ii} X_i^2 + \sum_{i=1}^{n} \sum_{j>1}^{n} \beta_{ij} X_i X_j \quad (6.2)$$

where Y denotes the predicted response, total experimental runs were denoted by n, while β_o= constant, β_i= linear, β_{ii}= quadratic, and β_{ij}= interaction term regression coefficients, respectively. Further, using Design Expert software, the fitness of the regression model was investigated using ANOVA and regression analysis at a 95% confidence level.

6.5 Pyrolysis Experimental setup

The pyrolysis setup and details of the experimental procedure were presented in Fig. 3.2. For each run, 10±0.5 g of SB feedstock was kept in the reactor for a residence time of 45 minutes. The yield of bio-oil, biochar, and non-condensable gases, was computed using the formulae below:

$$\text{Bio-oil yield (wt.\%)} = \frac{\text{Bio-oil weight}}{\text{Biomass weight}} \text{x} 100 \quad (6.3)$$

$$\text{Biochar yield (wt.\%)} = \frac{\text{Biochar weight}}{\text{Biomass weight}} \text{x}100 \quad (6.4)$$

$$\text{Gases yield (wt.\%)} = 100 - (\text{bio-oil yield} + \text{biochar yield}) \quad (6.5)$$

6.6 Physicochemical characterization of pyrolysis products

The pyrolysis products obtained after the experiment were characterized based on their physical properties, composition, and functional groups. Brookfield viscometer was employed to measure the viscosity of the pyrolytic liquid at 50 rpm and 30 °C. A pH meter (CL-54, Toshcon Industries Pvt. Ltd. Ajmer) was used to know the acidity of the SB's biochar and bio-oil. Bomb calorimeter (RSI Company, New Delhi, India) was used to find out the calorific value of the raw biomass and pyrolysis products. The density of the bio-oil was measured with a volumetric flask and weighing machine. The qualitative and quantitative analysis of bio-oil was done employing gas chromatography-mass spectroscopy (Agilent 5977B GC/MSD) which was furnished with HP-5MS column (30 m × 0.25 mm id with 0.25-micron film thickness). The system is programmed such that sample analysis was done at 40°C for 30 seconds which was further enhanced from 10 °C /min to 300°C. The instrument was set to run for a total of 30 min. 1.0 µl bio-oil sample was inserted, and the carrier gas (helium) flow rate was maintained to 0.6 ml/min. NIST library was used to classify the compounds and their composition by using the obtained chromatograph at different retention time and mass spectra. Fourier transform infrared spectroscopy (Model: Nicolet iS5, Thermo Electron Scientific Instruments LLC) based on attenuated total reflection (ATR) mode was employed to classify different functional groups present in the bio-oil. The physicochemical characterization (proximate analysis, ultimate analysis, higher heating value (HHV), and bulk density) of SB biochar has been analyzed using the same procedure as adopted for raw biomass. The surface morphology of the biochar was accomplished using a field emission scanning electron

microscope (FE-SEM, Nova Nano SEM 450) coupled with energy dispersive X-ray spectrometer (EDX).

6.7 Results and discussion

6.7.1 Characteristics

Physicochemical characterization of SB biomass is given in Table 6.1 and has been related to earlier reported biomasses like maple leaf waste [157], sugarcane leaves [144], *Acacia nilotica* [132], pistachio shell [158]. The proximate analysis results established that SB biomass has lower moisture content. Earlier studies suggested that biomass with a moisture content of less than 10% is appropriate for pyrolysis [157,159]. The heating value of the fuel diminishes as the moisture content increases. Furthermore, excessive moisture content leads to increased fuel consumption, resulting in significant volumes of flue gas. SB biomass has high volatile matter and lowers ash content. Biomass with a high volatile matter content is highly reactive and may ignite at very low temperatures. Biomass with higher content in volatiles are also suitable for gasification and higher bio-oil production [160]; however, lower ash has additional benefits. It reduces the problem of slagging and fouling during boiler operations and increases the fuel's higher heating value [95]. Fixed carbon content represents the applicability of the biomass towards various applications such as carbon nanotubes (CNTs), fertilizers, cosmetics, and bio-adsorbents. Ultimate analysis results established that SB biomass has higher carbon content and lower nitrogen content with negligible sulfur content. Higher carbon content causes higher energy content in the biomass feedstock. Low sulfur and nitrogen content causes lower emission of H_2S and NH_3 during the thermochemical conversion process. Lower sulfur content also diminishes the problem of corrosion in pipes and boilers [100]. The SB's higher heating value (HHV) is determined to be 21.82 MJ/kg, while its bulk density was 300.34 kg/m^3. A higher heating value is directly related to the carbon content of the biomass. Higher the carbon content, the higher the HHV of the fuel [63]. The fiber analysis of SB biomass such as

hemicellulose, cellulose, and lignin are presented in Table 6.1. In addition, the energy content of the SB biomass was described by employing the Van-Krevelen diagram (Fig. 6.1). The molar ratios (O/C and H/C) have been compared with maple leaf waste [157], *Pinus ponderosa* [7], *Acacia nilotica* [132], pistachio shell [158]. From Fig. 6.1, it can be seen that the O/C and H/C ratio of SB biomass was higher than coal, whereas it is comparable to other testified biomass.

Table 6.1: Physicochemical characteristics of SB biomass along with other reported biomass

Analysis	*Sesbania bispinosa*	Maple leaf waste [157]	Sugarcane leaves [144]	*Acacia nilotica* [132]	Pistachio shell [158]
Proximate analysis (wt. %)					
Moisture[a]	6.30±0.70	6.28	5.67	6.46	5.72
Volatile matter[b]	79.35±1.34	81.20	77.33	79.08	79.80
Ash content[b]	3.95±0.49	6.12	6.38	0.78	1.97
Fixed Carbon[b, c]	10.4	6.40	10.67	13.68	12.51
Ultimate analysis (%)					
Carbon[b]	54.64±0.67	49.40	76.83	43.69	45.31
Hydrogen[b]	6.60±0.5	4.32	8.19	7.54	5.49
Nitrogen[b]	0.71±0.05	1.98	0.59	0.47	0.28
Oxygen[b, c]	38.05	44.14	14.39	48.30	48.92
Sulfur[b]	–	0.16	–	–	–
O/C ratio	0.52	0.67	0.14	0.83	0.81
H/C ratio	1.45	1.04	1.28	2.07	1.45
Fiber analysis (wt. %)					
Hemicellulose[b]	23.9±0.87	–	42	28.64	21.55
Cellulose[b]	47.2±1.33	–	44	41.66	51.18
Lignin[b]	17.42±1.04	–	17	24.20	21.51
Extractives[b, c]	11.7	–	–	5.50	5.76
Calorific value[b] (MJ/kg)	21.82±1.10	16.32	18.08	18.66	16.85
Bulk density[a] (kg/m^3)	300.34±2.7	–	–	–	–

[a] Wet basis; [b] Dry basis; [c] By difference

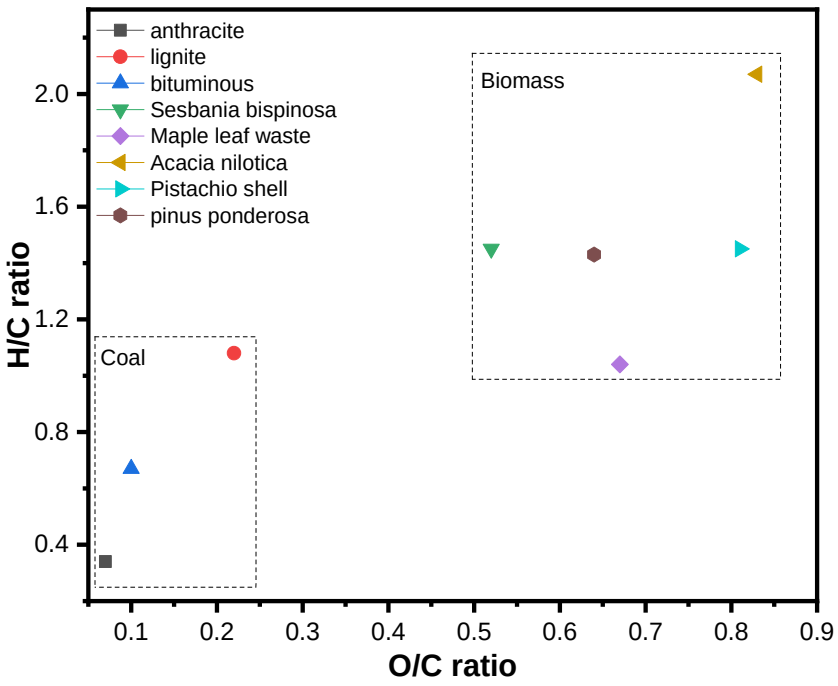

Fig. 6.1: Van-Krevelen diagram for SB with other testified biomass

6.7.2 FTIR study of SB

FTIR spectroscopy in the wavenumbers (400 – 4000 cm^{-1}) was employed to see the different functional groups attached to the SB biomass (Fig. 6.2). The absorption band at 3393 cm^{-1} was due to –OH stretching of water, phenols, and alcohols [100,161]. The peak at 2919 cm^{-1} is ascribed to symmetric and asymmetric vibrations of mainly alkanes, whereas the stretching mode of carbonyls, primarily ketones, and esters, was responsible for the peak of 1738 cm^{-1}. Peak (1647 cm^{-1}) is responsible for the carbonyl group of hemicellulose, while aromatic ring of lignin is responsible for the peak at 1501 cm^{-1} [110]. The peak confirmed the existence of hemicellulose and cellulose at 1438 cm^{-1}; however, the peak at 1371 cm^{-1} confirmed groups of aromatic methoxyl. Carbohydrate functional groups such as cellulose and hemicellulose are responsible for the peaks at 1246 and 1061 cm^{-1}. Peak (607 cm^{-1}) is attributed to the existence of the C–C aromatic ring [110].

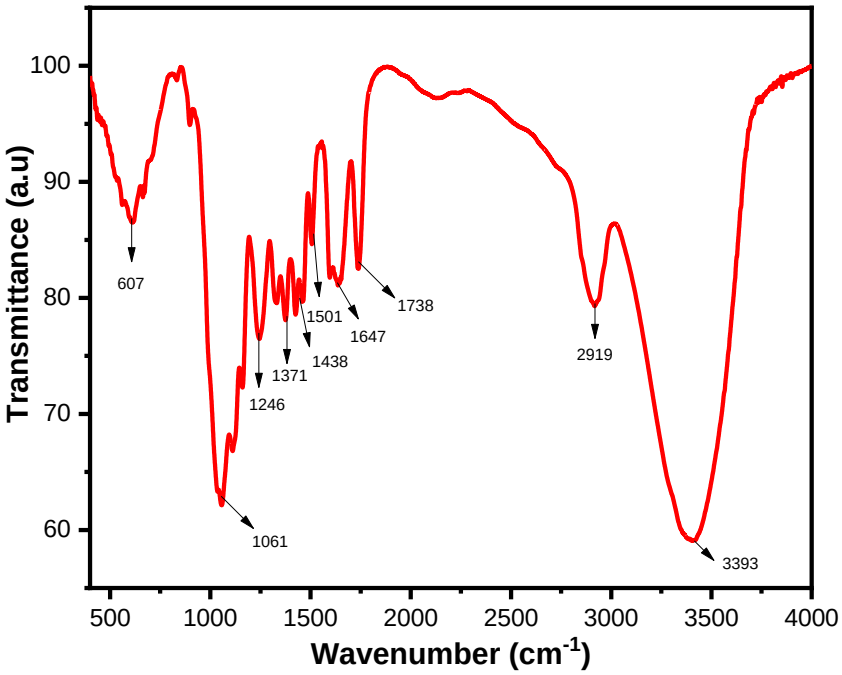

Fig. 6.2: FTIR analysis of SB biomass

6.7.3 Thermal analysis

The thermal stability of SB biomass was performed in a thermogravimetric analyzer at 10 °C/min, while its thermal decomposition profile is displayed in Fig. 6.3 (a). Fig. 6.3 (a) portrayed that the thermal profile of SB is divided into three main stages. The first stage ranges from 18 to 134.65°C, corresponding to drying; the second stage ranges from 134.65 to 726.81°C, corresponding to the active pyrolysis stage; and the third stage ranges from 726.81 to 1000°C, which corresponds to passive pyrolysis stage [88]. The first step corresponds to the removal of inbound moisture and certain low molecular weight volatile components of SB biomass, resulting in a weight loss of 7.58%. The main stage of the pyrolysis process, also known as the devolatilization phase, starts from 134.65°C and continues upto 726.81°C with a weight loss of 88.85%. The weight loss in this stage corresponds to higher removal of volatiles due to deterioration of hemicellulose, cellulose, and some parts of lignin. With continuous exposure to heat, higher molecular weight compounds (i.e., oligomeric components from the depolymerisation of hemicellulose, cellulose, and lignin) are depolymerized to lower molecular weight compounds such as phenols, acids, aldehydes, ketones, etc. The active pyrolytic stage

is further divided into three main sub-stages. A similar study was also reported by Cai et al., [162] and Huang et al., [160]. The first subdivision ranges from 134.65 to 297.56°C, mainly attached to the degradation of hemicellulose. The second subdivision ranges from 297.56 to 398.26°C, corresponding to deterioration of cellulose and partial lignin. The third subdivision ranges from 398.26 to 726.81°C, corresponding to deterioration of remaining lignin and other complex organic compounds that were even more strenuous than the first and second sub-stage. The degradation of lignin is more complex than hemicellulose and cellulose due to its higher thermal stability. Earlier studies suggested that hemicellulose, cellulose, and lignin degraded in the temperature range of 215 – 315°C, 315 – 450°C, and 200 – 900°C, respectively [163]. A similar temperature range was also noticed in the present study with small variations due to inherent structural characteristics, variety, and composition of biomass. The passive pyrolysis zone (>726.81°C) explicated further no mass loss, although inorganic residue was observed in the form of carbon and ash.

The DTG thermograph also revealed that SB biomass is pyrolyzed in three main steps. The first peak was discovered at 59°C due to the exclusion of moisture and light molecular weight compounds. Further, hemicellulose shoulder occurred at 297.56°C, and the cellulose peak was found at 327°C, while the lack of a peak in the decomposition of lignin can be attributed to its sluggish rate of decomposition. The highest weight loss for the SB biomass was observed to 0.43 mg/min at 327°C.

6.7.4 Effect of heating rate

The effect of dynamic heating rates on SB biomass is portrayed in Fig. 6.3 (b and c). It can be observed from Fig. 6.3 (b and c) that with an upsurge in heating rates (10 to 50 °C/min), TG and DTG thermographs switched to higher temperature regions without destroying the thermal degradation pattern. This increase in heating rate creates instability as biomass reaches a higher temperature in a shorter span of time. Fig. 6.3 (b) shows that TGA thermographs of SB biomass

shifted to higher temperature regions (230, 239, 252, 259, and 273°C) with an upsurge in heating rates from 10 to 50 °C/min, respectively. Ahmad et al., [157] and Mishra et al., [95] also found a similar profile with an increase in heating rates. Ahmad et al., [157] performed pyrolysis of maple leaf waste in a thermogravimetric analyzer (10 to 40 °C/min) in an N_2 environment. They reported that the TGA curve moved to a higher temperature region deprived of damaging the thermal profile. Mishra et al., [95] pyrolyzed *Phyllanthus emblica* kernel and *Azadirachta indica* fruit in a thermogravimetric analyzer (10 to 50 °C/min). They observed that the TGA thermograph moved to a higher temperature region without destroying the thermal degradation pattern. The relocation of TG thermograph towards higher temperature province was due to rise in degradation temperature of the biomass as heating rate raised. At a lower heating rate, heat transfer limitation was minimum in contrast to a higher heating rate. At higher heating rates, degradation occurs slowly due to heat transfer constraints resulting in uneven heating among biomass, whereas a slower heating rate causes uniform heating of biomass, and biomass interacts longer duration in the reactor, resulting in maximum heat transfer among them [95]. It is noticed that the degradation rate enhanced with an increase in heating rate due to supplement thermal energy. It was also mentioned that volatile matters were little affected at higher heating rates. The percent weight loss in the active zone was found to be 88.85, 86.56, 72.1, 70.76, and 66.34% with respect to heating rates of 10, 20, 30, 40, and 50 °C/min. This happened due to the creation of temperature lag by the biomass thermal resistance towards the radial direction, resulting in the higher charring. Further, at higher heating rates (30, 40, and 50 °C/min), point of inflection was missing as in the case of lower heating rates (10 and 20 °C/min). There was a continuous reduction in mass loss % with temperature. This was due to a rise in the development of active species as a result of the thermal degradation of cellulose. These active species interact among themselves and with lignin, the progressive degradation of lignin that leads to the formation of char [110]. At the end of the experiment, the leftover

inorganic residue increases by 2.80, 3.03, 8.53, 13.81, and 17.51%, with an increase in heating rate (10, 20, 30, 40, and 50 °C/min). This was because, at a lower heating rate, residence time was high that causing complete interaction among biomass (complete pyrolysis), resulting in lower inorganic residue [7].

Further, burnout temperature was reported by various earlier researchers to understand the combustion behavior of the fuel [7,110]. It can be explained as the temperature at which the weight loss rate declines steadily to less than 1 percent per minute. Burnout temperature for the SB biomass is found to be 405, 416, 431, 450, and 460°C at a heating rate of 10 to 50 °C/min respectively.

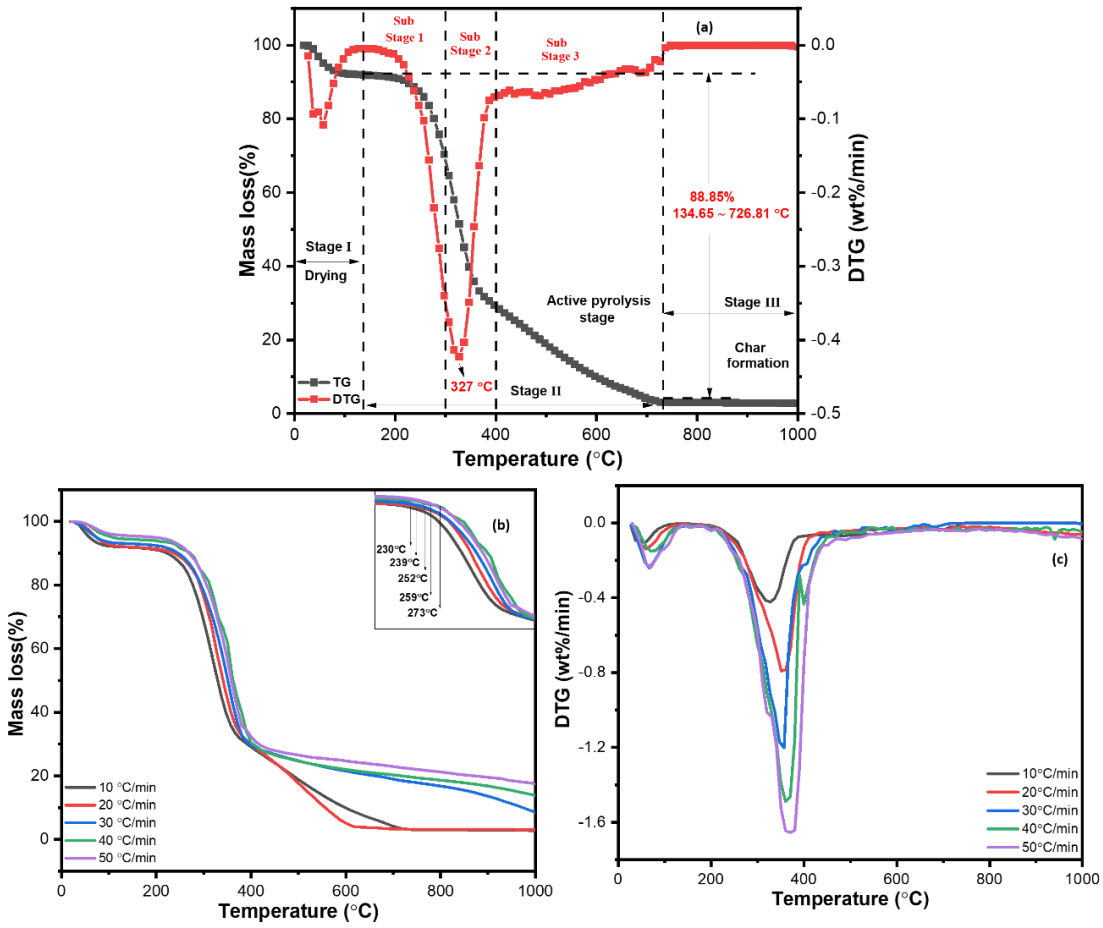

Fig. 6.3: (a) Thermal analysis of SB at 10 °C/min, **(b)** TG profile at dynamic heating rates, and **(c)** DTG thermograph at dynamic heating rates

6.7.5 Kinetic analysis using model-free methods

The kinetic analysis of the SB biomass was estimated in the conversion range of 0.1 to 0.8 using the isoconversional plot as seen in Fig. 6.4, based on the model-free methods of KAS, OFW, TM, ST, and VZK method that is presented in Table 6.2. The conversion value above 0.8 was not used due to poor fitting of the data and low correlation coefficient [95]; however, the correlation coefficient value obtained in the conversion range (0.1 to 0.8) was greater than 0.91 for every model that demonstrated the right fit to the experimental data. The activation energy values altered from 81.74 to 225.19 kJ/mol, 77.49 to 224.57 kJ/mol, 77.83 to 224.9 kJ/mol, 77.77 to 224.88 kJ/mol and 72.34 to 204.19 kJ/mol, whereas average values of the activation energies are 181.37, 180.63, 180.91, 180.90, and 161.31 kJ/mol engaging OFW, KAS, TM, ST, and VZK method respectively. Activation energy is defined as the bare lowest energy necessary to initiate a process or reaction. Lower activation energy indicates a faster reaction [7]. Furthermore, the physical relevance of the activation energy from the isoconversional approaches is minimal. However, molecular collision theory can be used to understand this approach. This theory explains that, during random pyrolysis, just a few particular molecules were impacted, which increased their kinetic energy and allowed them to start reactions that broke prior chemical bonds [95]. Furthermore, the reactivity of any fuel has a significant influence on pyrolysis; it may be estimated from the activation energy [95]. It aids in the optimization of various process factors and the creation of a new pyrolyzer [7]. The variation of activation energy corresponding to conversion is portrayed in Fig. 6.5. The activation energy of SB biomass pyrolysis changed with an increase in conversion, indicating the presence of complicated multi-step reactions such as parallel, competitive, and consecutive reactions. This change in activation energy with conversion is due to a difference in the thermal breakdown temperature range of the primary chemical elements of biomass (hemicellulose, cellulose, and lignin) [95,107]. It is observed that activation energy values increased from conversion 0.1 to 0.6, whereas it started to decline from 0.7 to 0.8. The increasing trend of

activation energy with conversion may be attributed to the exothermic nature of the breakdown process, which is frequently influenced by competing macromolecules and intermolecular companions. The decrease in activation energy with conversion indicated the endothermic nature of the reaction followed by an irreversible step [87]. At the initial stages of conversion, activation energy is lower due to the requirement of lower energy for the removal of moisture and some very light components in the SB biomass. As the conversion progressed, the activation energy increased because of higher energy consumption for the degradation of hemicellulose and cellulose components of the SB biomass. The pyrolysis of hemicellulose is dominant in the conversion range (0.2 – 0.3) and requires less activation energy than cellulose. Since hemicellulose is less thermally stable, it has a lower degree of polymerization than cellulose. Hemicellulose is mainly composed of blends of xylose, galactose, mannose, glucose, and arabinose due to the polymerization of different monosaccharides. The degradation of cellulose starts from 0.3 to 0.4 and requires even more energy than hemicellulose. Degradation of cellulose is more strenuous than hemicellulose because of its high crystallinity and ordered microfibrils; cellulose has a long linear chain attached to the D-glucosyl group [162]. Lignin degraded over a wide temperature range. In the conversion range of 0.6 to 0.8, deterioration of major lignin and other complex organic compounds was even more strenuous than in the first and second sub-stage. The degradation of lignin is more difficult than hemicellulose and cellulose due to its high thermal stability. The high thermal stability of lignin is due to the attachment of phenolic hydroxyl group and cross-linking of hemicellulose and cellulose. In addition, it should be noted that biomass with a higher cellulose and hemicellulose content decomposed faster and produced a more significant fraction of gaseous products. A higher lignin content leads to a slower decomposition, a lower product gas yield, and a higher temperature where devolatilization kicks in [164].

Further, little variation in activation energy estimates between models is attributable to the adaption of various kinds of assumptions by the respective models. Furthermore, differences in biomass chemical constituents, complicated processes, and charring all have a part in the activation energies value variation [105,107]. Shape, size, and fiber content, such as cellulose, hemicellulose, and lignin content, have a very high impact on the variation of activation energy [97]. In addition, every feedstock has its unique disintegration temperature range, and activation energy is totally a temperature-dependent quantity. Less temperature and energy are required to disintegrate fragile bonds, whereas high temperature and energy are required for stronger bonds [95]. Furthermore, the inherent mineral content of a similar type of biomass is altered by the nature of the soil and the climatic circumstances in which it is cultivated. Ashutosh et al., [165] have already demonstrated that the addition of metal (Ru and Fe) lowers the activation energy. Activation energy may differ based on the kind of biomass or even for the same biomass obtained from different locations [110]. Researchers reported that the activation energy of biomass has a direct relationship with fuel kinds, mathematical computations, and pyrolysis experiments (operating parameters). Among the different models employed to analyze TGA data in this work, the Vyazovkin models do not avail any mathematical assumptions [110]. Hence it is more appropriate to evaluate the kinetic parameters employing the VZK method as no approximation errors are involved. ICTAC, an advanced isoconversional organization, also supports our findings, claiming that VZK surpasses alternative model-free techniques[95]. Aside from VZK, KAS has the most error rate, followed by OFW, ST, and TM, owing to imposed assumptions.

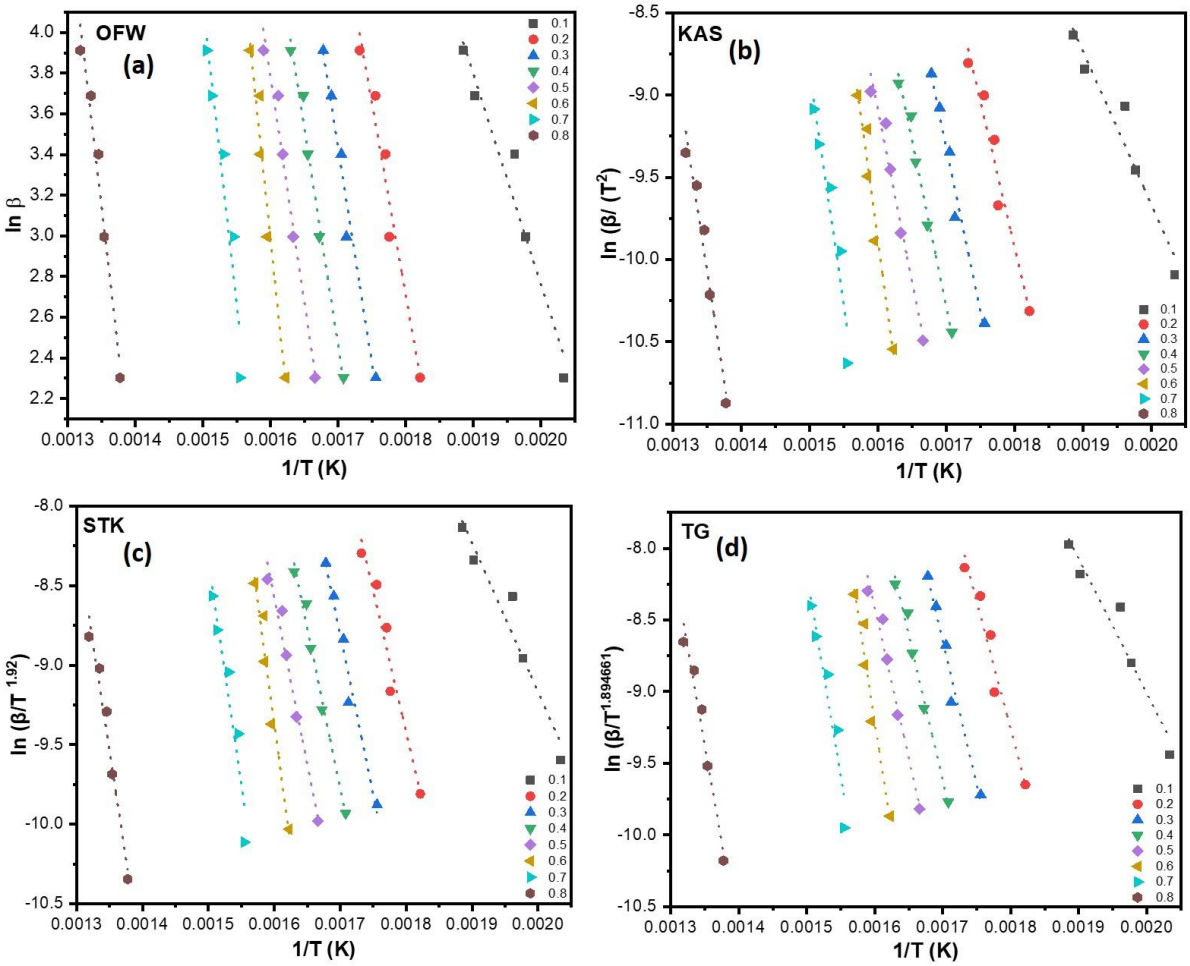

Fig. 6.4: Curve fitting of pyrolysis of SB against model-free methods

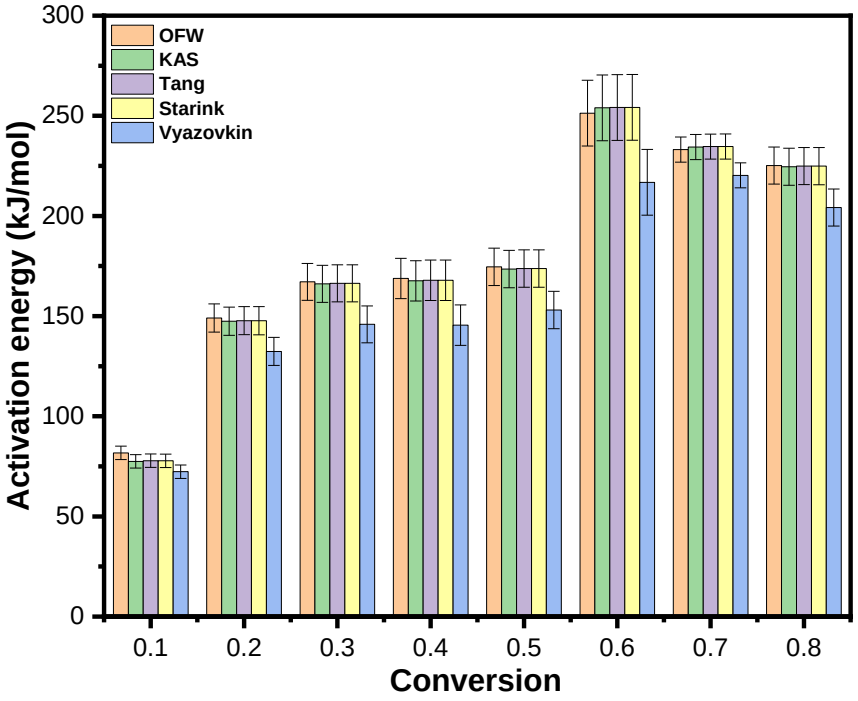

Fig. 6.5: Variation of activation energy with progressive conversion

Table 6.2: Activation energy with respect to conversion obtained from different model free techniques

(α)	OFW	R^2	TM	R^2	KAS	R^2	ST	R^2	VZK
	E(kJ/mol)		E(kJ/mol)		E(kJ/mol)		E(kJ/mol)		E(kJ/mol)
0.1	81.74	0.9519	77.83	0.9417	77.49	0.9410	77.77	0.9415	72.34
0.2	149.06	0.9556	147.74	0.9504	147.46	0.9501	147.72	0.9503	132.38
0.3	167.1	0.9745	166.38	0.9717	166.11	0.9716	166.37	0.9717	145.90
0.4	168.8	0.9855	167.89	0.9838	167.61	0.9837	167.88	0.9838	145.51
0.5	174.6	0.9745	173.76	0.9716	173.47	0.9714	173.74	0.9715	153.07
0.6	251.32	0.9553	254.16	0.9519	253.98	0.9517	254.19	0.9519	216.81
0.7	233.16	0.9220	234.64	0.9155	234.41	0.9151	234.66	0.9154	220.28
0.8	225.19	0.9698	224.9	0.9666	224.57	0.9664	224.88	0.9666	204.19
Mean	181.37	−	180.91	−	180.63	−	180.90	−	161.31

6.7.6 Master plot

Pyrolysis of biomass is a highly complex process that involves a number of series and parallel reactions simultaneously. As a result, determining the response mechanism of such a complicated process is extremely difficult. A mechanistic model based on appropriate mathematical approximation has been created to anticipate the response mechanism of such complicated processes. In this study Criado z(α) master plot was used to predict the reaction mechanism at all heating rates to see the effect of heating rate on the reaction model followed during pyrolysis. Fig. 6.6 (a - f) portrayed the z(α) master plot at all heating rates, whereas the functions f(α) and g(α) are given in (Table – 3.1). At lower heating rates (10 and 20 °C/min) and in the conversion of 0.1 – 0.2, the experimental curve crosses over most of the different theoretical curves such as F1, F2, D2, D3, R1, R2, R3, A2, A3, P2, P3 and P4 deducing the complex reaction mechanism followed by the SB biomass during pyrolysis. Hence it is very difficult to predict the exact mechanism in the conversion 0.1 – 0.2; however, in between 0.2 to 0.5 conversion, the experimental curve follows F2 and F3 theoretical curves that correspond to random nucleation with two and three nuclei on the individual particle, respectively. At higher heating rates (30 and 40 °C/min) and lower conversion values (0.1 to 0.4), the experimental curve crosses over different theoretical curves such as F1, D2, D3, R1, R2, R3, A2, A3, P2, P3, and P4. Hence it is very difficult to predict the exact mechanism of this conversion, whereas, in the conversion range of 0.4 to 0.5, the experimental curve (30 °C/min) and (40 °C/min) follows F1 and D4 theoretical curve that corresponds to random nucleation with one nuclei on the individual particle and three-dimensional diffusion mechanism respectively. For the highest heating rate (50 °C/min) and in between 0.1 to 0.2 conversion range, the experimental curve follows P4 and D4 theoretical curves that correspond to power law and three-dimensional diffusion mechanism, respectively, whereas in the conversion range, 0.2 to 0.4 it crosses over D1 and D4 theoretical curves that correspond to diffusion

mechanism in one and three-dimension. The conversion range of 0.4 to 0.5 overlapped the D1 theoretical curve that follows the diffusion mechanism in one dimension. At a higher conversion value ($\alpha>0.5$) and all heating rates, the experimental curve is closed to the D3 theoretical curve that corresponds to the three-dimensional diffusion mechanism. According to the earlier reported data, biomass components decomposed into smaller molecules at greater than 50% conversion owing to increased temperature [95]. This behavior might potentially be ascribed to broken cellulose being accelerated not just by diffusion but also by diffusion of hot gases produced throughout the specimen. In addition, at a lower conversion value ($\alpha<0.5$), the character of the plot changed dramatically, implying that with change in heating rate, different response mechanisms have been followed. It can be inferred from the above investigation that at a lower conversion value, the prediction of a solid response mechanism is extremely difficult.

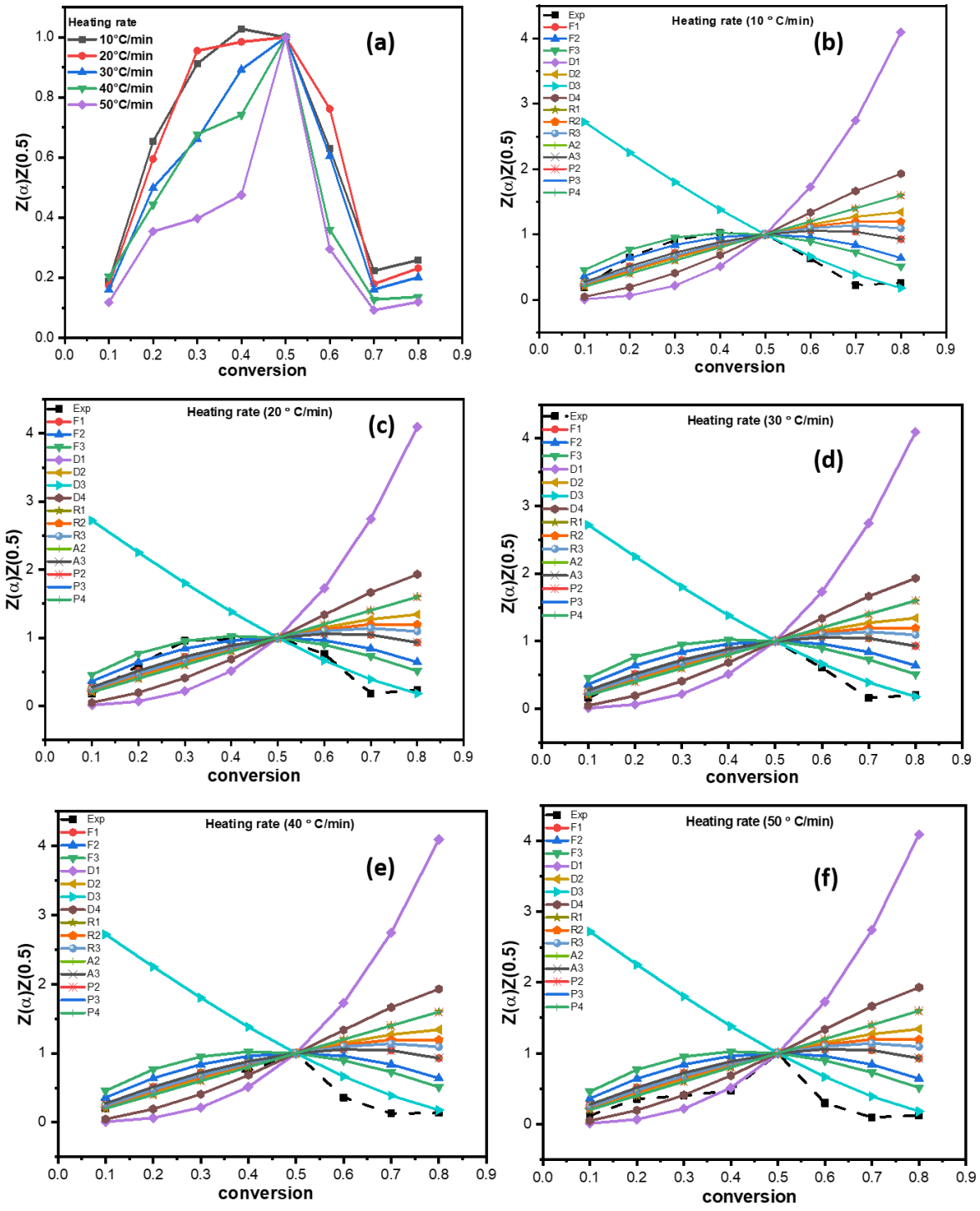

Fig. 6.6: (a) z(α)z(0.5) with progressive conversion at various heating rates; **(b)** at 10 °C/min; **(c)** 20 °C/min; **(d)** 30 °C/min; **(e)** 40 °C/min; and **(f)** 50 °C/min

6.7.7 Thermodynamic analysis

The thermodynamic analysis was carried out at five different heating rates (10, 20, 30, 40, and 50 °C/min) to see how the heating rate influenced thermodynamic features (Table 6.3). The frequency factor in the conversion range 0.1 to 0.8 altered from 1.676997E+6 to 1.41387E+19,

7.7365124E+5 to 1.8484E+18, 7.60121E+5 to 1.6766E+18, 6.33647E+5 to 1.00146E+18 and 5.30201E+5 to 6.05258E+17 at heating rates of 10, 20, 30, 40 and 50 °C/min employing OFW technique respectively, whereas it gets altered from 2.255841E+5 to 1.90578E+17, 1.13033E+5 to 2.9966E+16, 1.11639E+5 to 2.75006E+16, 9.51198E+4 to 1.72479E+16 and 8.13055E+4 to 1.09327E+16 at heating rates of 10 to 50 °C/min employing VZK technique respectively. The average value of the frequency factor obtained from OFW and VZK method was 3.81768E+20, 3.98775E+19, 3.56615E+19, 2.00777E+19, 1.14547E+19 and 9.87339E+17, 1.36607E+17, 1.24359E+17, 7.54117E+16, 4.62561E+16 at heating rates of 10 to 50 °C/min respectively. The development of a chemical complex in SB biomass prior to the synthesis of end products is indicated by the extremely high value of the pre-exponential factor ($>10^9$ s^{-1}). This is due to intricate parallel chemical reactions throughout the pyrolysis process. The change in enthalpy (ΔH) value in the conversion range 0.1 to 0.8 altered from 77.65 to 219.15 kJ/mol, 77.53 to 219.04 kJ/mol, 77.50 to 219.01 kJ/mol, 77.37 to 218.96 kJ/mol, and 77.33 to 218.88 kJ/mol at heating rates of 10 to 50 °C/min employing OFW technique respectively, whereas it gets altered from 68.25 to 198.15 kJ/mol, 68.13 to 198.04 kJ/mol, 68.10 to 198.01 kJ/mol, 67.96 to 197.96 kJ/mol, and 67.93 to 197.88 kJ/mol at heating rates of 10 to 50 °C/min employing VZK technique respectively. The average change in enthalpy (ΔH) values obtained from OFW and VZK method was 176.40, 176.30, 176.27, 176.22, 176.16 kJ/mol, and 156.34, 156.24, 156.21, 156.16, 156.11 kJ/mol at heating rates of 10 to 50 °C/min respectively. The variation in enthalpy with conversion followed a similar pattern of alteration in activation energy with conversion for SB pyrolysis. Further, the positive value of enthalpy indicated that energy was required to fragment the biomass, indicating that the pyrolysis reaction is endothermic in a nitrogen atmosphere. The difference between enthalpy and activation energy is very little (~5). This demonstrates that the potential energy barrier is easily exceeded during the pyrolysis of SB biomass, and the product created is feasible. The Gibb's

free energy value altered from 160.70 to 155.64 kJ/mol, 168.59 to 163.31 kJ/mol, 168.95 to 163.65 kJ/mol, 171.06 to 165.69 kJ/mol, and 173.16 to 167.73 kJ/mol at heating rates of 10 to 50 °C/min employing OFW technique respectively, whereas it gets altered from 161.31 to 156.13 kJ/mol, 169.23 to 163.82 kJ/mol, 169.59 to 164.16 kJ/mol, 171.70 to 166.20 kJ/mol, and 173.82 to 168.25 kJ/mol at heating rates of 10 to 50 °C/min employing VZK technique respectively. The average value of Gibb's free energy obtained from the OFW and VZK method was 156.96, 164.69, 165.04, 167.09, 169.15 kJ/mol, and 157.56, 165.32, 165.67, 167.72, 169.79 kJ/mol at heating rates of 10 to 50 °C/min respectively. The change in ΔG with conversion reveals that there is enough energy in the pyrolysis reaction at the attitude of the reagent by producing the activated complex. It may be optimized to address the variations in heat flow and its disorder [166]. It is also an important feature of the state used to anticipate the severity and frequency of the reactions. The change in Gibb's free energy demonstrated that the overall energy of the reaction mechanism increased from the point of the reagents to the creation of the activated complex. Furthermore, a larger value of Gibbs free energy indicates a reduced possibility of reaction with an intense evaluation of heat flow and disorder change [112]. A positive value of ΔG indicates that the reaction is non-spontaneous and must be completed with the addition of supplementary energy. The degree of randomness in the system is signified by a change in entropy (ΔS). The obtained ΔS value is negative between 0.1 to 0.5 conversions; however, it is positive in the conversion range of 0.6 to 0.8. The positive value of entropy suggested that the products formed by bond dissociations have a higher degree of disorderness than the reactants, whereas the negative value indicates its opposite [6]. The significant change in entropy led the material towards the physicochemical aging process, eventually putting it close to the thermodynamic equilibrium. In this case, the material exhibited low reactivity and increased the time required to make the activity complicated. Further, the obtained results of the thermodynamic parameters are matched with the earlier

reported biomass of finger millet straw [167], mustard straw [117], pigeon pea stalk [168], *Arundo donax* biomass [159], *Vachellia nilotica* weed [169], pearl millet [170], Musa balbisiana trunk [110], *Azadirachta indica* [95], and *Phyllanthus emblica* [95]. The alteration among the thermodynamic properties of the different biomass was due to differences in the chemical constituents of biomass, inherent mineral content, nature of the soil, and the climatic conditions where they have grown [110].

Table 6.3: Thermodynamic analysis of the SB biomass

β (°C/min)	Conversion	A(1/sec)	ΔH(kJ/mol)	ΔG(kJ/mol)	ΔS(J/mol.K)	A(1/sec)	ΔH(kJ/mol)	ΔG(kJ/mol)	ΔS(J/mol.K)
		OFW				VZK			
10 °C/min	0.1	1.676997E+6	77.65	160.70	-138.37	2.255841E+5	68.25	161.31	-155.06
	0.2	2.21275E+12	144.49	157.70	-22.00	6.943543E+10	127.82	158.29	-50.78
	0.3	9.22005E+13	162.36	157.13	8.71	1.1497E+12	141.16	157.80	-27.73
	0.4	1.30947E+14	163.93	157.08	11.41	1.06041E+12	140.64	157.82	-28.62
	0.5	4.33106E+14	169.60	156.91	21.15	5.07561E+12	148.08	157.57	-15.81
	0.6	2.96769E+21	246.19	155.09	151.79	2.53835E+18	211.69	155.83	93.06
	0.7	7.23128E+19	227.81	155.47	120.53	5.16978E+18	214.93	155.75	98.60
	0.8	1.41387E+19	219.15	155.64	105.82	1.90578E+17	198.15	156.13	70.01
	Mean	3.81768E+20	176.40	156.96	32.38	9.87339E+17	156.34	157.56	-2.04
	M.D	6.46481E+20	40.98	1.18	70.25	1.43336E+18	38.93	1.24	66.94
	STD	9.77666E+20	50.63	1.66	87.07	1.78211E+18	46.58	1.69	80.39
	Variance	9.5583E+41	2563.73	2.75	7582.68	3.17593E+36	3170.36	2.87	6463.80
20 °C/min	0.1	7.7365124E+5	77.53	168.59	-145.07	1.13033E+5	68.13	169.23	-161.06
	0.2	5.64871E+11	144.37	165.46	-33.58	2.052457E+10	127.69	166.08	-61.14
	0.3	2.00855E+13	162.24	164.86	-4.17	3.01761E+11	141.04	165.57	-39.07
	0.4	2.81031E+13	163.82	164.81	-1.56	2.79283E+11	140.53	165.58	-39.90
	0.5	8.83307E+13	169.51	164.63	7.76	1.25083E+12	147.98	165.32	-27.62
	0.6	3.08358E+20	246.10	162.73	132.83	3.57215E+17	211.59	163.50	76.62
	0.7	8.81409E+18	227.78	163.12	103.00	7.05675E+17	214.89	163.42	82.01
	0.8	1.8484E+18	219.04	163.31	88.80	2.9966E+16	198.04	163.82	54.53
	Mean	3.98775E+19	176.30	164.69	18.50	1.36607E+17	156.24	165.32	-14.45
	M.D	6.71201E+19	41.00	1.24	67.28	1.97419E+17	38.95	1.30	64.13
	STD	1.01516E+20	50.65	1.73	83.40	2.4423E+17	46.60	1.77	77.02
	Variance	1.03055E+40	2565.43	3.00	6956.60	5.96482E+34	2171.90	3.14	5932.28
30 °C/min	0.1	7.60121E+5	77.50	168.95	-145.27	1.11639E+5	68.10	169.59	-161.22
	0.2	5.34565E+11	144.36	165.81	-34.06	1.960473E+10	127.68	166.43	-61.55
	0.3	1.88178E+13	162.22	165.21	-4.74	2.86074E+11	141.02	165.92	-39.55
	0.4	2.63045E+13	163.78	165.16	-2.19	2.64822E+11	140.49	165.94	-40.42
	0.5	8.24108E+13	169.46	164.98	7.11	1.18108E+12	147.93	165.67	-28.18

	0.6	2.75655E+20	246.07	163.08	131.84	3.2553E+17	211.56	163.85	75.79
	0.7	7.95945E+18	227.73	163.47	102.07	6.41839E+17	214.85	163.77	81.14
	0.8	1.6766E+18	219.01	163.65	87.94	2.75006E+16	198.01	164.16	53.76
	Mean	3.56615E+19	176.27	165.04	17.83	1.24359E+17	156.21	165.67	-15.02
	M.D	5.99984E+19	41.00	1.24	67.08	1.79663E+17	38.95	1.30	63.94
	STD	9.07455E+19	50.64	1.73	83.16	2.22194E+17	46.60	1.77	76.79
	Variance	8.23475E+39	2565.05	3.08	6916.17	4.93703E+34	2171.65	3.16	5897.92
40 °C/min	0.1	6.33647E+5	77.37	171.06	-147.02	9.51198E+4	67.96	171.70	-162.78
	0.2	3.81091E+11	144.32	167.87	-36.95	1.452855E+10	127.64	168.50	-64.11
	0.3	1.28645E+13	162.18	167.27	-7.98	2.05445E+11	140.98	167.98	-42.37
	0.4	1.79118E+13	163.76	167.22	-5.42	1.90356E+11	140.47	168.00	-43.20
	0.5	5.53655E+13	169.44	167.04	3.77	8.3418E+11	147.91	167.73	-31.10
	0.6	1.54953E+20	246.07	165.11	127.05	1.98266E+17	211.56	165.88	71.67
	0.7	4.66704E+18	227.66	165.5	97.54	3.87778E+17	214.78	165.80	76.85
	0.8	1.00146E+18	218.96	165.69	83.59	1.72479E+16	197.96	166.20	49.82
	Mean	2.00777E+19	176.22	167.09	14.32	7.54117E+16	156.16	167.72	-18.15
	M.D	3.37188E+19	41.00	1.26	66.30	1.08805E+17	38.95	1.32	63.19
	STD	5.10004E+19	50.66	1.76	82.22	1.34389E+17	46.62	1.80	75.93
	Variance	2.60104E+39	2567.38	3.10	6761.17	1.80604E+34	2173.75	3.24	5765.56
50 °C/min	0.1	5.30201E+5	77.33	173.16	-148.58	8.13055E+4	67.93	173.82	-164.16
	0.2	2.73728E+11	144.26	169.94	-39.81	1.083776E+10	127.58	170.57	-66.66
	0.3	8.86981E+12	162.14	169.33	-11.13	1.48627E+11	140.95	170.05	-45.13
	0.4	1.23023E+13	163.69	169.28	-8.64	1.37832E+11	140.41	170.07	-45.98
	0.5	3.75296E+13	169.36	169.09	0.425	5.93745E+11	147.84	169.80	-34.04
	0.6	8.82618E+19	246.02	167.14	122.3	1.22127E+17	211.51	167.93	67.56
	0.7	2.77014E+18	227.63	167.54	93.16	2.36989E+17	214.76	167.84	72.72
	0.8	6.05258E+17	218.88	167.73	79.30	1.09327E+16	197.88	168.25	45.93
	Mean	1.14547E+19	176.16	169.15	10.87	4.62561E+16	156.11	169.79	-21.22
	M.D	1.92018E+19	41.00	1.27	65.53	6.66509E+16	38.95	1.33	62.46
	STD	2.90442E+19	50.66	1.78	81.26	8.22202E+16	46.62	1.82	75.05
	Variance	8.43564E+38	2567.23	3.17	6604.68	6.76015E+33	2173.51	3.32	5632.68

Note: MD = Mean deviation, STD = Standard deviation

6.7.8 Compensation effect

The interaction effect between pre-exponential factors and activation energy is shown in Fig. 6.7 It shows that there is a compensation effect between the activation energy and pre-exponential factor with respect to conversion level (R^2 closes to 1). At the molecular level, an escalation in temperature enhances particle quivering, resulting in increased stretching and bending of molecules. Furthermore, the nucleation reaction diminishes when the biomass porosity increases and the diffusion process takes control at higher temperatures. The interaction between the pre-exponential factor and activation energy is linear because the reaction rate is expected to satisfy an Arrhenius-rate law. The linear pattern depicted by the plot (Fig. 6.7) validated the accuracy of the kinetic parameters calculated in this study.

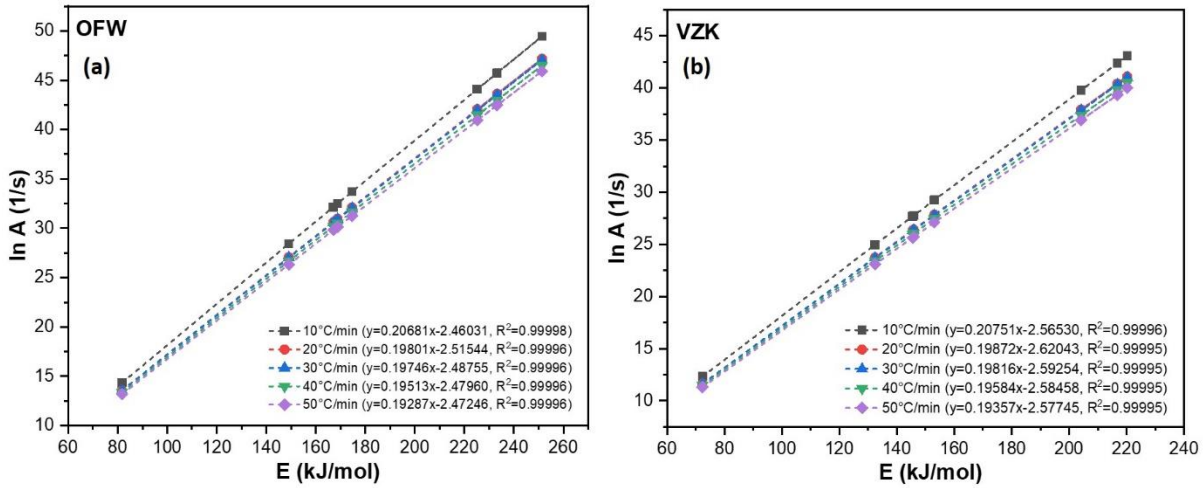

Fig. 6.7: Correlation between pre-exponential factor and activation energy; **(a)** OFW and **(b)** VZK method

6.7.9 Pyrolysis parameter optimization using RSM

Response surface methodology (RSM) based on the central composite design (CCD) approach was employed to investigate the simultaneous influence of process response and independent factors. The process response selected in this investigation was bio-oil yield, with temperature, heating rate, and N_2 flow rate as independent variables. 19 experimental runs were carried out as per the suggestion of design expert software which comprises of 6, 8, and 5 axial, factorial, and center points, respectively. The detailed experimental design matrix and responses are

presented in Table 6.4. The relationship between the dependent factor and the independent factors was represented by coded factors as given below:

$$Bio-oil\ yield\ (wt\ \%) = +37.10 + 3.68A + 0.1459B + 0.0430C + 2.46A^2 - 1.20B^2 - 0.4582C^2 - 0.0212AB - 0.0787AC + 0.0413BC$$

where the coded factors such as A, B, and C denotes temperature, heating rate, and N_2 flow rate. The bio-oil yield varied from 34.02 to 42.53%; however, the optimal temperature, heating rate, and N_2 flow rate for the highest bio-oil yield were 585°C, 60°C/min, and 125 ml/min. The results of ANOVA are presented in Table 6.5. F and p-value can be used to assess the impact of each independent variable on the response at a 95% confidence interval. The significance of any model is to be decided on the basis of high F and low p-value. The F and p-value for the current study are 1096.16 and <0.0001 for bio-oil yield, respectively, indicating that the generated model is appropriate. By combining the linear and quadratic components, it is possible to conclude that factors A, B, A^2, B^2, and C^2 were notable since the value of p was less than 0.0500 (Table 6.5). The individual term of C, and interaction terms (AB, BC, and AC) are non-significant (higher p-value). The larger F-value corresponding to temperature (6736.91) than the heating rate (10.73) and N_2 flow rate (0.9425) deduced that temperature has a considerable influence on the yield of liquid than the N_2 flow rate and heating rate. Brown et al., [118] and Kiliç et al., [80] reported a similar result. Further, it was also noted that the interaction terms such as AB, AC, and BC didn't impact the yield of bio-oil due to lower F-values. Hence these terms are regarded as minimal or inconsequential. The F-values of A^2, B^2, and C^2 were obtained to be 367.04, 76.16, and 6.13, indicating that A^2 (temperature) influences pyrolytic liquid output. The findings indicated that the N_2 flow rate had no discernible effect on the bio-oil yield. Fig. 6.8 depicts the relationship between the actual and expected values. The results revealed that the actual value is extremely close to the anticipated value with an R^2

value of 0.9991, indicating that the selected model was successful and competent for understanding the effects of the pyrolysis process.

The purpose of a three-dimensional plot is to categorize the surface form for various factors used and to show the efficacy of the various variables on the bio-oil yield [116]. The contour plot of the close-fitting model is the most meaningful and straightforward way to define the feather of the response surface. Furthermore, limiting the number of process variables to two or three simplifies the production and comprehension of contour plots [80,118]. The present study deals with the effect of three process parameters on the yield of pyrolysis products. Representing all the effects in the same three-dimensional and counter plots is nearly impossible. As a result, one parameter was held constant while others were changed. The impact of process variables such as temperature, heating rate, and N_2 flow rate on the bio-oil yield is portrayed in Fig. 6.9 (a, b, and c). It can be seen from Fig. 6.9 (a) that as the temperature increased from 300 to 585°C, bio-oil yield enhanced; however, with any further increase, it started to decline. From the same Fig. 6.9 (a), it can be seen that, with a rise in heating rate from 40 to 60°C/min, bio-oil yield enhanced; with any further increment, it started to decline. Similar results were also obtained from the corresponding contour plot. Fig. 6.9 (b) portrayed the effect of temperature and N_2 flow rate on bio-oil yield. The effect of temperature on bio-oil yield has been discussed. It is clear from the figure that, with an increase in N_2 flow rate from 50 to 125 ml/min, bio-oil yield is enhanced; with any further increase it gets decreased. Fig. 6.9 (c) portrayed the effect of heating rate and N_2 flow rate on the yield of bio-oil. It can be seen from the Fig. 6.9 (c) that when the heating rate increased from 40 to 60°C/min, the bio-oil production increased; however, as the heating rate increased further, the yield began to fall. On the other hand, increasing the N_2 flow rate from 50 to 125 ml/min increased bio-oil yield, however any further increase lowered it. Further, it was found from the Fig. 6.9 (a, b, and c)

that the influence of temperature was larger than the heating rate and N_2 flow rate, while the impact of the N_2 flow rate was negligible in comparison to temperature and heating rate.

Table 6.4: CCD experimental matrix and results

Run	Factor 1	Factor 2	Factor 3	Response	Response
	A: Temperature	B: Heating rate	C: Gas flow rate	Bio-oil yield	Bio-oil yield
	°C	°C/min	ml/min	Actual (%)	Predicted (%)
1	450	60	150	36.92	37.07
2	300	80	50	34.19	34.23
3	450	60	100	36.85	37.04
4	450	60	125	37.19	37.10
5	585	60	125	42.53	42.40
6	600	40	50	41.52	41.54
7	600	80	200	41.68	41.71
8	300	80	200	34.58	34.56
9	450	60	125	37.15	37.10
10	450	60	125	37.13	37.10
11	600	80	50	41.74	41.70
12	450	40	125	35.72	35.76
13	450	65	125	37.13	37.07
14	450	60	125	37.22	37.10
15	300	40	50	34.02	33.98
16	300	40	200	34.11	34.14
17	585	60	125	42.23	42.40
18	450	60	125	37.15	37.10
19	600	40	200	41.43	41.38

Table 6.5: ANOVA analysis of the quadratic model

Source	Sum of Squares	df	Mean Square	F-value	p-value	
Model	158.93	9	17.66	1096.16	< 0.0001	significant
A-Temperature	108.53	1	108.53	6736.91	< 0.0001	
B-H.R	0.1729	1	0.1729	10.73	0.0096	
C-Gas flow rate	0.0152	1	0.0152	0.9425	0.3570	
AB	0.0036	1	0.0036	0.2242	0.6471	
AC	0.0496	1	0.0496	3.08	0.1132	
BC	0.0136	1	0.0136	0.8450	0.3820	
A^2	5.91	1	5.91	367.04	< 0.0001	

B^2	1.23	1	1.23	76.16	< 0.0001	
C^2	0.0988	1	0.0988	6.13	0.0352	
Residual	0.1450	9	0.0161			
Lack of Fit	0.0947	4	0.0237	2.35	0.1865	not significant
Pure Error	0.0503	5	0.0101			
Cor Total	159.07	18				
R^2	0.9991					
Adjusted R^2	0.9982					
Predicted R^2	0.9741					

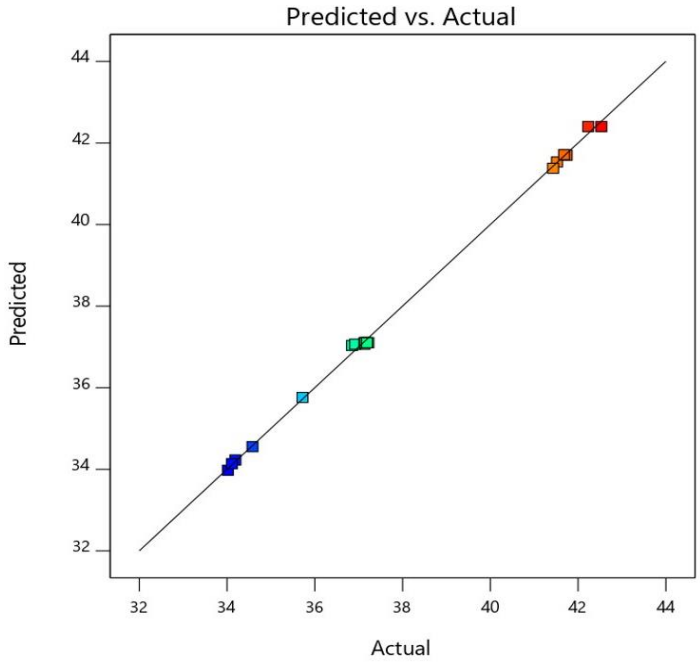

Fig. 6.8: Actual and predicted values of the SB bio-oil

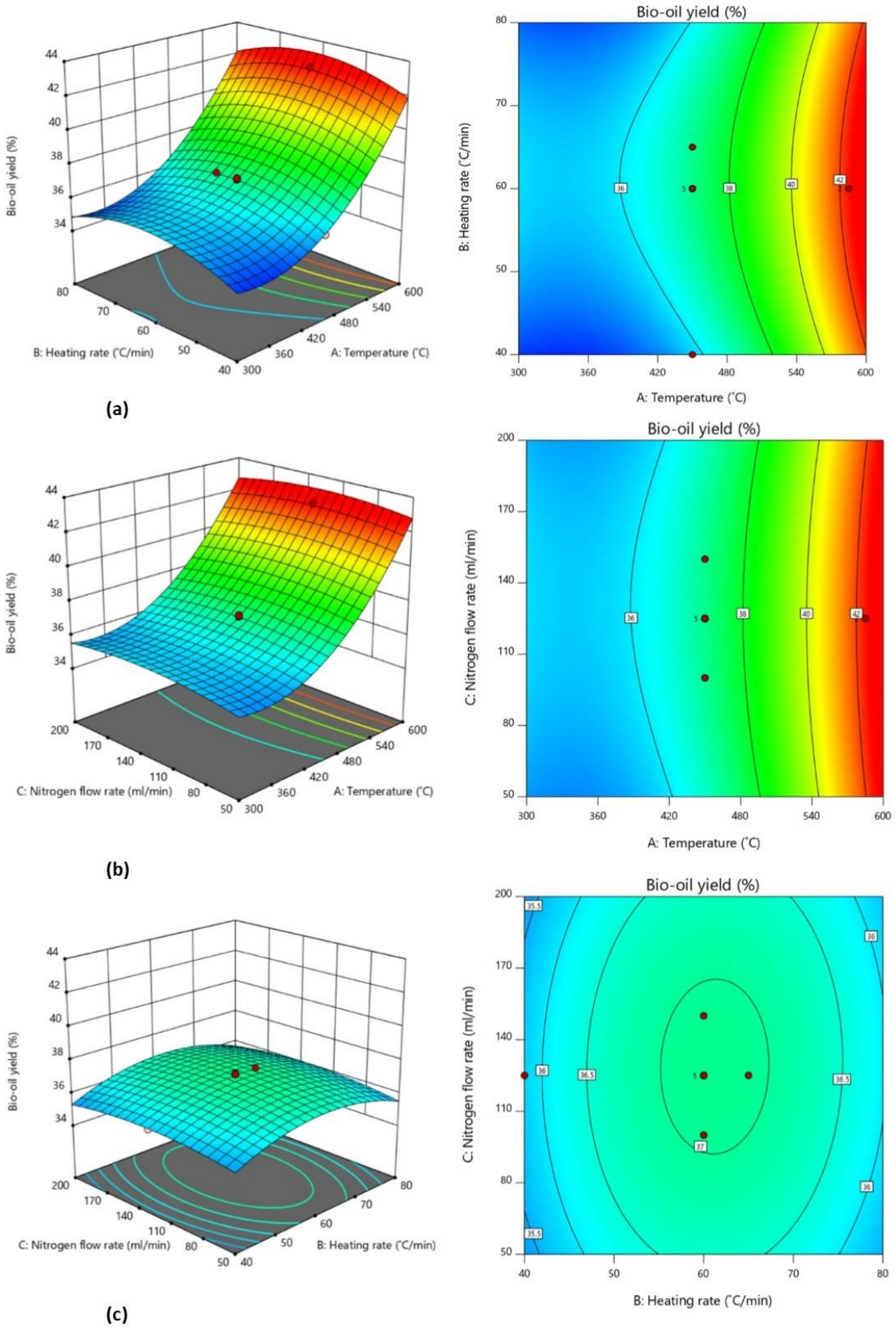

Fig. 6.9: Effects of the surface response of bio-oil yield in three dimensions, **(a)** temperature and heating rate, **(b)** N_2 flow rate and temperature, and **(c)** N_2 flow rate and heating rate

6.7.10 Bio-oil characterization

Bio-oil obtained after pyrolysis of SB was characterized based on their physicochemical characterization and has been compared with diesel fuel [171]. The details of the results are presented in Table 6.6. The bio-oil has a dark brown and smoky smell. The pH of the bio-oil was found to be very low (2.65). The low pH negatively impacts the HHV of the bio-oil, making it extremely corrosive, with its severity reaching severe levels at high temperatures [172]. The viscosity of the bio-oil was found to be 6.14 cSt, higher than diesel fuel. Viscosity directly impacts flame temperature, stability, fluidity, design, and injection of fuel [117,119]. It is reported that if the volatiles is not allowed to escape during storage, the viscosity of the bio-oil rises with time, which can be linked to an increase in molecular weight [173]. Furthermore, the unsaturated oxygen may promote polymerization processes, increasing the viscosity of the pyrolytic oil over time [62]. The density of bio-oil is an important metric during combustion since it represents the quality of atomization, fluidity, vaporization, ignition, and combustion properties [174]. The density of the bio-oil was found to be 940.66 kg/m^3, whereas the HHV of the bio-oil was found to be lower (16.96 MJ/kg). The low HHV of the SB bio-oil was due to its higher acidity. The ash content of the bio-oil was found to be 0.81%. Finally, the ramsbottom carbon residue of the bio-oil was found to be 1.85 wt. %.

Table 6.6: Physicochemical characterization of SB bio-oil and compared with diesel fuel

Analysis	SB bio-oil	Diesel
Colour	Dark brown	–
Smell	Smoky	–
Acidity	2.65±0.008	–
Density(kg/m^3)	940.66±4.04	828
Viscosity (cSt) (30 °C) (50 rpm)	6.14±0.09	2 – 4.5
Ash Content (wt. %)	0.81±0.015	–
HHV (MJ/kg)	16.96±0.17	45.5
Ramsbottom carbon residue (wt. %)	1.85±0.06	–

6.7.11 FTIR analysis of the bio-oil

The FTIR spectroscopy (Fig. 6.10) was employed to find the attachment of different functional groups to the bio-oil. The occurrence of phenols, water, protein, alcohol, and aromatics was revealed by the absorption band 3360 cm^{-1} attributable to –OH stretching vibrations [6,100]. Peak 2942 cm^{-1} is attributed to symmetric and asymmetric vibrations of principally alkanes, whereas peak 1708 cm^{-1} is attributed to the stretching mode of carbonyls, particularly ketones and esters [110]. The peak at 1636 cm^{-1} is responsible for the carbonyl group of hemicellulose, while the peak at 1523 cm^{-1} is due to the aromatic ring of lignin. The absorption band between 1460 – 1375 cm^{-1} confirmed the existence of –CH bending vibration, indicating the presence of alkanes [62]. The presence of ester functionalities was confirmed by the adsorption band 1106 – 1010 cm^{-1} caused by C–O–C stretching vibration. The presence of mono and polycyclic aromatic compounds in the bio-oil accounts for the peaks at 677 cm^{-1} [117].

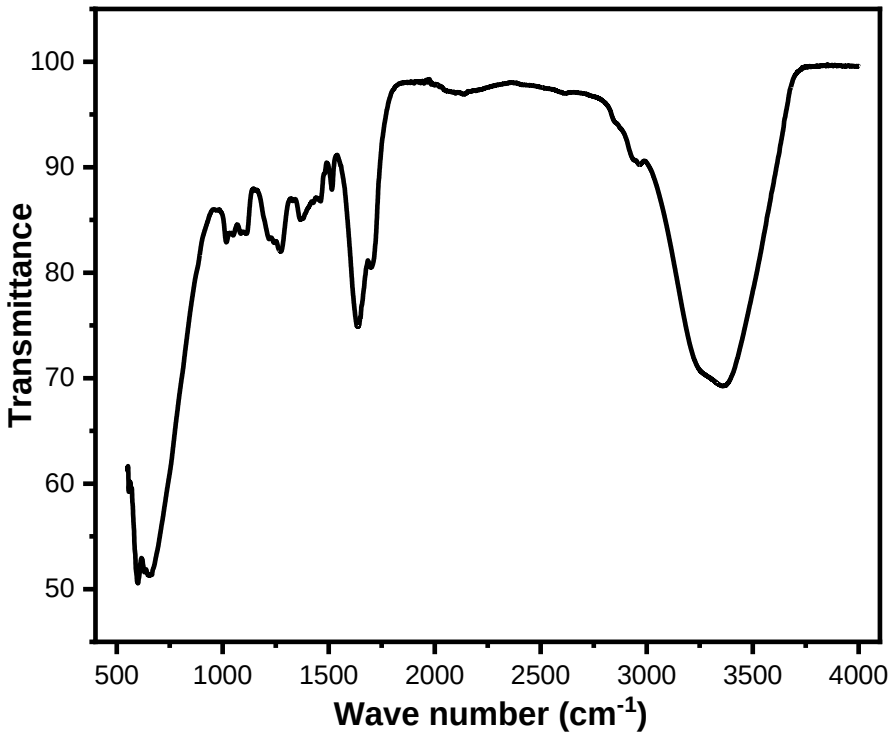

Fig. 6.10: FTIR analysis of SB bio-oil

6.7.12 GCMS analysis

The bio-oil was subjected to gas chromatography-mass spectroscopy (GCMS). The resulting mass spectra were compared to the NIST library database in order to identify the unknown organic compounds present in the bio-oil, as shown in Fig. 6.11. The detailed chemical list is presented in Appendix F. It is reported that bio-oil comprises different types of oxygenated and non-oxygenated compounds, including hydrocarbons, acids, ketones, aldehydes, esters, ethers, amides, nitriles, alcohols, phenols etc. [65]. It can be seen from Fig. 6.11 that bio-oil has hydrocarbons (37.77%), acids (10.85%), esters (14.67%), ketones (14.82%), alcohols (4.06%), amides (8.41%), phenols (0.68%), nitrogen-containing compounds (1.28%) and other compounds (7.46%). These compounds have different commercial and industrial applications. Further, it is noticed that oxygenated compounds are higher in bio-oil, which has a detrimental influence when the primary objective of the bio-oil is for transportation fuel. Hence upgrading bio-oil using catalytic pyrolysis becomes necessary.

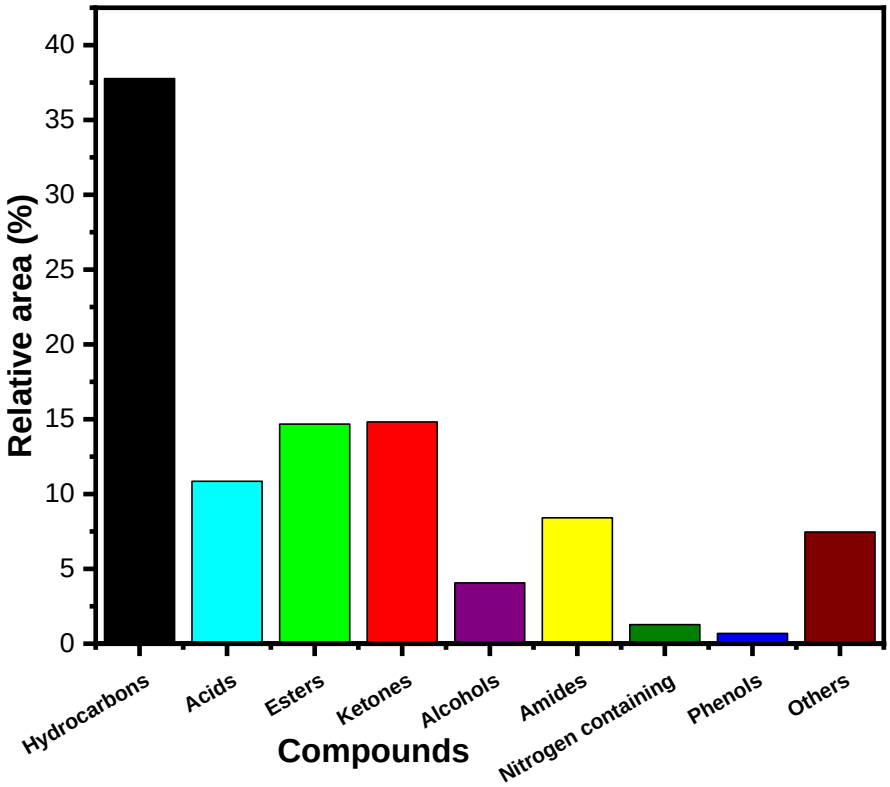

Fig. 6.11: GCMS analysis of the bio-oil

6.7.13 Characterization of biochar

The solid material, also called biochar, left in the reactor has been characterized based on its physicochemical characterization. Biochar offers a number of different applications in industries as well as in agriculture. The physicochemical characterization results of SB biochar, along with the reported results of *Manilkara zapota* seed biochar [62], pea nut shell biochar [68], and coal [62], are presented in Table 6.7. The proximate analysis results confirmed lower moisture (4.6%), volatile matter (21.2%), and ash content (5.65%), whereas fixed carbon content was higher (68.55%), which has several industrial applications. Biochar having lower moisture and ash content has higher ignition efficiency. Lower moisture content also causes longer storage of biochar [129]. It is reported that lower ash content causes lower slagging and fouling problems during boiler operations. Further, higher ash content caused a lower calorific value of biochar and acted as a heat sink. The ultimate analysis results confirmed higher carbon (67.56%), lower hydrogen (1.93%), and lower nitrogen (0.36%). Lower nitrogen content has both advantages and disadvantages. Lower nitrogen of biochar causes lower NOx problems during combustion, whereas lower nitrogen content in biochar also has limited application when the primary objective of the biochar is to use it in soil enhancement [131]. From the results, it is also clear that carbon content rose and oxygen content reduced considerably. This occurs as a result of decarboxylation, dehydration, and deoxygenation of raw SB after pyrolysis. The biochar's higher heating value was obtained to be 26.03 MJ/kg., substantially higher than the raw biomass (21.82 MJ/kg). This rise in HHV value following pyrolysis was connected to changes in carbon and oxygen content. The transportation and ease of storage are represented through bulk density which was found to be 450.36 kg/m^3. Surface area is an important parameter for employing biochar as an adsorbent. The biochar's BET surface area was determined to be 210.26 m^2/g, lower than activated carbons (800 m^2/g). The zeta potential of the biochar was found to be -31.3 mV, whereas the acidity of the biochar was found to be 9.40. Furthermore, the influence of molar ratios (O/C and H/C) was examined using Van-

Krevelen diagram (Fig. 6.12 (a)). Biochar with lower O/C and H/C ratios has excellent fuel properties because of the reduction in energy loss, smoke, and water vapor while burning. The H/C and O/C ratio of the SB biochar was compared with *Manilkara zapota* seed biochar [62], pea nut shell biochar [68], *Samanea saman* seed biochar [63], palm shell hydrochar [129], coffee husk biochar [98], torrefied *Acacia nilotica* [132], *Lagerstroemia speciosa* seed hull biochar [88], and coal char [62]. It was found that SB biochar has lower O/C and H/C ratios compared to other biochars except for peanut shell biochar and coffee husk biochar. The lower molar ratios revealed the higher energy content of the SB biochar. In addition, the surface morphology of the SB biochar was studied using FE-SEM coupled with EDX, as portrayed in Fig. 6.12 (b). The results revealed that C and O are the major components of biochar, with additional elements of N, Mg, Na, P, Al, Si, Ca, and K. These mineral matters act as a catalyst in the pyrolysis process. The morphology of the biochar altered significantly due to deposition of various mineral components (EDX analysis). This happens due to several reactions (dehydration, decarbonylation, and decarboxylation) occurred during pyrolysis, altering the surface shape of biochar [134]. Moreover, a long channel were noticed as a result of the breakdown of chemical bonds, which is primarily responsible for the change in the structure of the biochar.

Table 6.7: Physicochemical characterization of SB biochar along with other reported biochars

Analysis	SB biochar	*Manilkara zapota* seed biochar [62]	Pea nut shell biochar [68]	Coal [62]
Proximate analysis (wt. %)				
Moisture	4.6±0.005	2.56	1.12	–
Ash Content	5.65±0.21	10.62	10.96	–
Volatile matter	21.2±0.98	25.32	10.45	–
Fixed carbon*	68.55	61.5	78.59	–
Ultimate analysis (wt. %)				
C	67.56±1.34	52.59	81.65	55.38
H	1.93±0.02	3.58	3.14	5.86
N	0.36±0.01	2.37	1.67	2.48
S	–	–	–	2.21

O*	30.15	41.46	13.54	34.07
O/C	0.33	0.59	0.12	0.46
H/C	0.20	1.04	0.15	1.27
Heating value (MJ/kg)	26.03±0.77	24.76	–	22.54
Bulk density (kg/m^3)	450.36±2.01	547	–	–
Acidity	9.40±0.14	9.49	–	–
BET surface area (m^2/g)	210.26	20.26	249.26	–
Zeta potential (mV)	-31.3±1.4	-30.97	–	–

*By difference

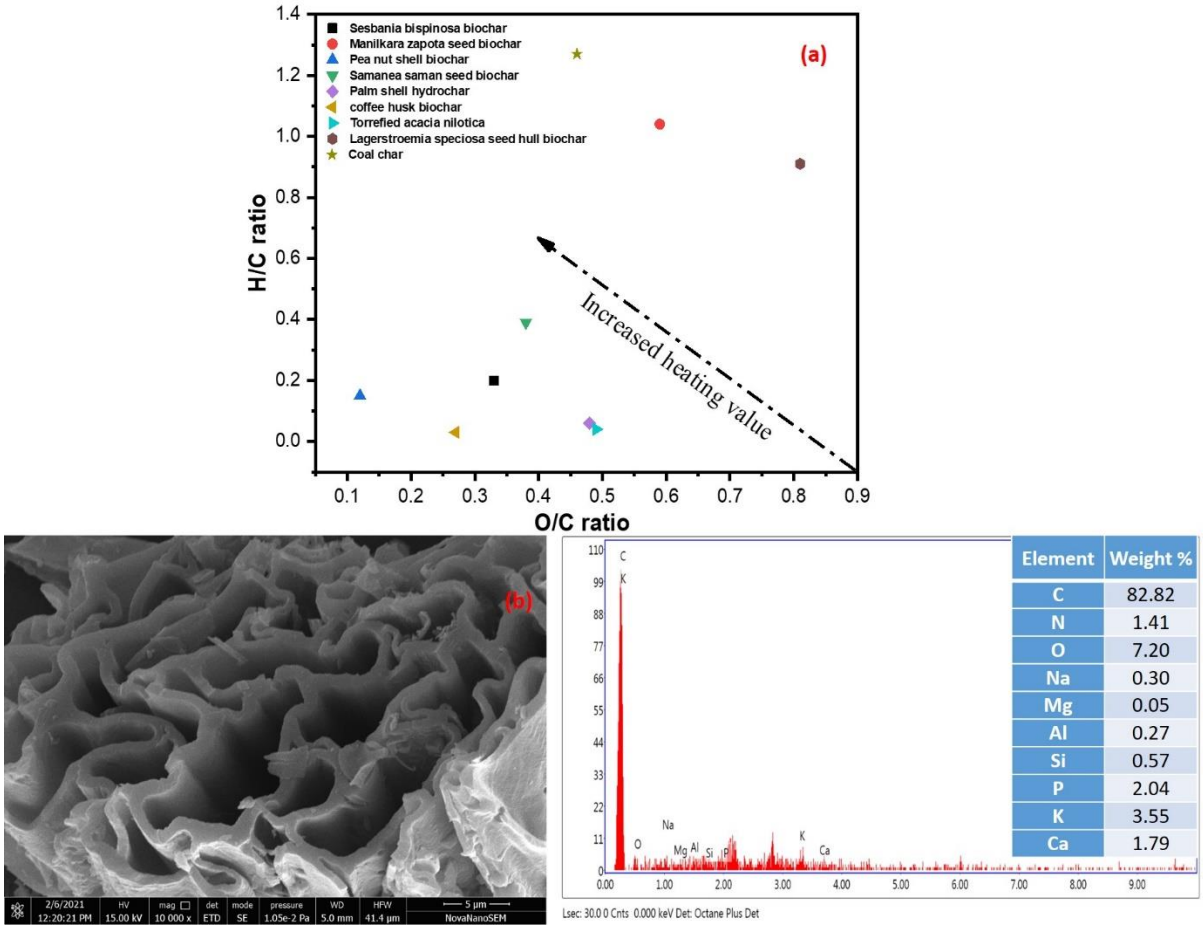

Fig. 6.12: (a) Van-Krevelen diagram, and **(b)** FE-SEM coupled with EDX of the SB biochar

6.8 Conclusion

The present study addressed the pyrolysis behavior of SB biomass to elucidate its bioenergy potential and applied RSM to optimize the important pyrolysis variables. The physicochemical

characterization results revealed tremendous bioenergy potential of SB with high carbon and volatile matter content. The thermogravimetric results revealed that major mass loss was found in the temperature range of 220 to 650°C, showing the optimal temperature range for the pyrolysis process. The kinetic analysis revealed that the apparent activation energy altered as the conversion progressed, indicating the complex and multistep process. The thermodynamic study revealed that the difference between E and ΔH is close to (~5 kJ/mol), implying that product formation can be accomplished by supplying very low supplemental energy. The master plot methodology was used in combination with the Criado method to estimate the reaction mechanism, which revealed a complex reaction mechanism with progressive conversion. ANOVA results revealed that temperature had a more promising impact on bio-oil yield than heating rate and N_2 flow rate. The optimum parameters (temperature = 585°C, heating rate = 60°C/min, and N_2 flow rate = 125 ml/min) for the highest bio-oil yield of 42.53 %. The characterization of the biochar revealed its applicability in multipurpose applications. The findings confirmed that SB biomass can be used as a substitute for conventional fuel through pyrolysis.